Nano Convergence

FULL PAPER

Open Access

Nanoscale inhomogeneity and the evolution of correlation strength in $FeSe_{1-x}S_x$

Yu Liu[1,3*], Aifeng Wang[1,4*], Qianheng Du[1,2,5], Lijun Wu[1], Yimei Zhu[1] and Cedomir Petrovic[1,2*]

Abstract

We report a comprehensive study of the nanoscale inhomogeneity and disorder on the thermoelectric properties of $FeSe_{1-x}S_x$ ($0 \leq x \leq 1$) single crystals and the evolution of correlation strength with S substitution. A hump-like feature in temperature-dependent thermpower is enhanced for $x = 0.12$ and 0.14 in the nematic region with increasing in orbital-selective electronic correlations, which is strongly suppressed across the nematic critical point and for higher S content. Nanoscale Se/S atom disorder in the tetrahedral surroundings of Fe atoms is confirmed by scanning transmission electron microscopy measurements, providing an insight into the nanostructural details and the evolution of correlation strength in $FeSe_{1-x}S_x$.

Keywords Thermoelectricity, Superconductivity, Electronic correlation, Disorder

1 Introduction

With a simple PbO-type structure FeSe shows a variety of complex and competing electronic phases [1], providing an ideal platform to probe the underlying physics of unconventional superconductivity (SC). Bulk FeSe is a compensated semimetal that exhibits SC with $T_c \approx 9$ K [2]; the T_c can be enhanced by applying physical pressure [3, 4], intercalation [5–9], ionic liquid gating [10], surface doping with alkaline metals [11, 12], isovalent S substitution in a modified hydrothermal growth [13], or in monolayer thin films on $SrTiO_3$ substrate [14–18]. Intriguingly, FeSe undergoes a tetragonal-to-orthorhombic structural (nematic) transition at $T_s \approx 90$ K without the formation of magnetic order [19–26]. This nematic phase is characterized by multiband shifts driven by orbital order that leads to Fermi-surface (FS) distortions, and it is additionally contributed by non-local Fe d_{xy} orbital besides a lifting of the degeneracy of the d_{xz} and d_{yz} states [26–28]. Furthermore, three gaps were determined in angle-resolved specific heat measurements [29]; strong electronic correlations was proposed by detecting a Hubbard-like band in FeSe [30].

Isovalent S substitution, which maintains the nature of compensated semimetals, is an effective route for tuning electronic states and correlations in FeSe. The nematicity is strongly suppressed with S substitution, and a nematic quantum critical point (NCP) appears at $x \approx 0.17$ [31–36]. The SC gap exhibits an abrupt change across NCP [32]; meanwhile, the normal state resistivity in the vicinity of NCP shows a linear temperature dependence [37–40], signifying non-Fermi-liquid behavior due to the nematic critical fluctuations. Strange metal component can also be observed in the Hall response of $FeSe_{1-x}S_x$ across the NCP [41]. Recent nuclear magnetic resonance (NMR) measurements revealed that antiferromagnetic (AFM) fluctuations

*Correspondence:
Yu Liu
liuyu002@mail.ustc.edu.cn
Aifeng Wang
afwang@cqu.edu.cn
Cedomir Petrovic
cedomir_petrovic@yahoo.com
[1] Condensed Matter Physics and Materials Science Department, Brookhaven National Laboratory, Upton, NY 11973, USA
[2] Department of Materials Science and Chemical Engineering, Stony Brook University, Stony Brook, NeY 11790, USA
[3] Center for Correlated Matter and School of Physics, Zhejiang University, Hangzhou 310058, China
[4] Present Address: College of Physics, Chongqing University, Chongqing 401331, China
[5] Present Address: Material Science Division, Argonne National Laboratory, Lemont, IL 60439, USA

show a positive correlation with T_c [42], although nematic fluctuations are most strongly enhanced near the QCP but without a clear correlation with the T_c [34]. Raman response from fluctuations was also studied [43, 44]. Additionally, quantum oscillation experiments indicated a topological Lifshitz transition and a reduction in electronic correlations across the NCP [45].

Thermopower is an effective probe to characterize the nature and sign of transport carries as well as the correlation strength in superconductors [46–54]. In addition, correlated quantum phases may also depend on nanoscale inhomogeneity [55]. Fundamentally, thermopower is entropy per carrier. Since it is directly related to the Fermi energy, thermopower measurement will assist in understanding the band structure. In cuprates, the FS reconstruction driven by the AFM order [56] and/or charge density wave [57, 58] have been revealed by thermopower measurement.

Here we investigated the evolution of electronic correlation strength and the Se/S atomic disorder in $FeSe_{1-x}S_x$ by the combination of scanning transmission electron microscopy, electrical and thermoelectric transport, Hall resistivity, and specific heat measurements. Strong nanoscale Se/S disorder appears in the middle range of $FeSe_{1-x}S_x$, away from the NCP. Our results indicate modest electronic correlations in FeSe and their significant reduction across the NCP, confirming an orbital selective correlation [59] and its weak connection to the nanostructural details.

2 Methods

High quality single crystals of $Fe_ySe_{1-x}S_x$ ($0 \le x \le 1$, $y \le 0.1$) were fabricated by the $AlCl_3$/KCl chemical vapor transport (CVT) method for $0 \le x \le 0.23$, and by the hydrothermal method for $0.4 \le x \le 1$, respectively, which are characterized as described previously [60–65] and labeled as $FeSe_{1-x}S_x$ ($0 \le x \le 1$) in this paper. High-resolution scanning transmission electron microscopy (STEM) imaging were carried out using the double aberration-corrected JEOL-ARM200CF microscope with high angle annular dark field (HAADF) detector and operated at 200 kV. The STEM-HAADF images were acquired with convergent semi angle of 21 mrad and collection semi angle from 67 to 275 mrad, respectively. The STEM samples were prepared by crushing the crystals and dispersed on a Lacy carbon TEM grid. The temperature-dependent in-plane resistivity ρ(T) and thermopower S(T) were measured in a quantum design PPMS-9 with standard four-probe technique. The relative error in our measurement for thermopower was below 5% based on Ni standard measured under the identical conditions. The heat capacity was measured by the heat pulse relaxation method in PPMS-9. The Hall resistivity ρ_{xy}(H) was measured using standard four-probe method with the current flowing in the *ab* plane and the magnetic field applied along the *c* axis. In order to effectively eliminate the longitudinal resistivity contribution due to voltage probe misalignment, the ρ_{xy}(H) was obtained by the difference of transverse resistance measured at positive and negative fields, i.e. $\rho_{xy} = [\rho_{+H} - \rho_{-H}]/2$. The sample dimensions were measured by an optical microscope Nikon SMZ-800 with 10 μm resolution.

3 Results and Discussion

High-resolution scanning transmission electron microscopy images recorded by high-angle annular dark-field detector (STEM-HAADF) indicate the presence of nanoscale inhomogeneity and strong disorder in the middle x range compared to FeSe and FeS [63]. The contrast of Se/S columns is weaker than that of Fe columns in high-S samples (Fig. 1a) and becomes stronger in high-Se samples [63]. From the refinement (Fig. 1b), we obtained that the full width at half-maximum (FWHM) values are 0.112(5) nm (Se/S peak) and 0.125(2) nm (Fe peak) for $FeSe_{0.06}S_{0.94}$, 0.106(3) nm (Se/S peak) and 0.112(2) nm (Fe peak) for $FeSe_{0.31}S_{0.69}$, and 0.116(4) nm (Se/S peak) and 0.124(3) nm (Fe peak) for $FeSe_{0.82}S_{0.18}$, respectively. We noted that the peak width of the atomic columns in STEM images depends on not only the disorder of the atomic position but also the probe size. The later may vary slightly due to the alignment of the microscope. To minimize the effect of the probe size variation, we calculate the normalized FWHM ($FWHM_{Se/S}/FWHM_{Fe}$). Figure 1(c) exhibits the normalized FWHM of Se/S columns, indicating that Se/S atomic positions are more disordered in the middle range of S doping at Se sites when compared to FeSe and FeS.

Figure 1(d,e) shows the temperature dependence of in-plane resistivity ρ(T) for $FeSe_{1-x}S_x$, typical metallic behavior over the entire temperature [63, 64]. The nematic transition temperature T_s determined by the minima of $d\rho/dT$ is $\sim$ 89 K for FeSe; it is monotonically suppressed by S substitution [Table 1], and is absent for $x = 0.23$ and higher x, arising from the suppression of orbital ordering by chemical pressure [66]. The residual resistivity ratio $RRR = \rho(300\ K)/\rho(14\ K)$ is $\sim$ 25 for FeSe, confirming low defect scattering and relatively high quality for vapor-grown FeSe crystals [67], which can be further optimized to $>$ 40 [68, 69]. As x is increased from 0, the value of RRR first decreases to 14.6 and 15.5 for $x = 0.12$ and $x = 0.14$, respectively, and then increases to 25.5 for $x = 0.23$ when T_s is completely suppressed (Fig. 1e). With increasing x, $FeSe_{1-x}S_x$ with $x = 0.4$ and 0.7 show rather small values of $RRR \sim 5$ and 8, respectively, due to the enhancement of anion height disorder-related scattering [63]. Then the RRR dramatically increases to $\sim$ 53.2 for pure FeS, higher than the reported 10 $\sim$ 46 for hydrothermal-synthesized

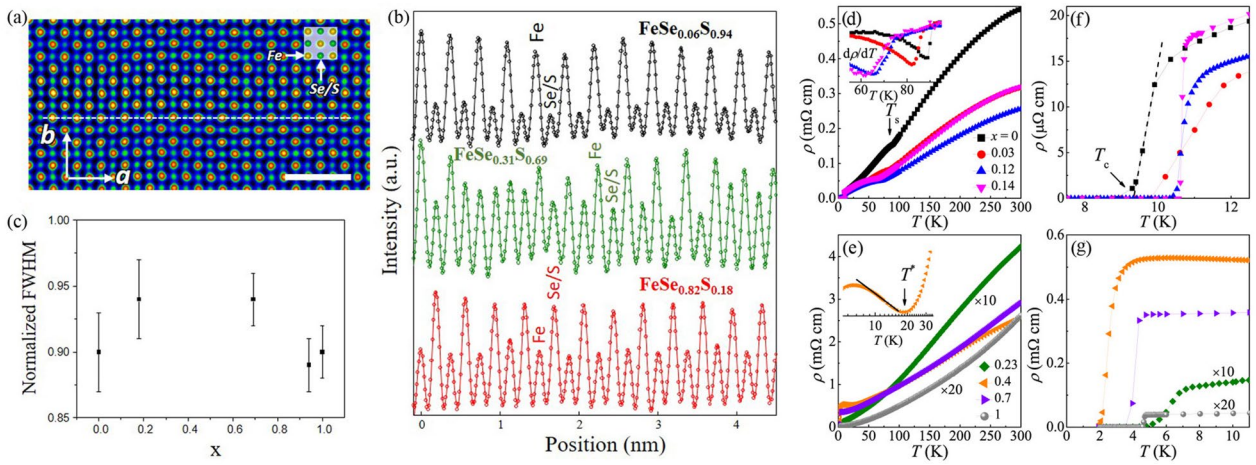

Fig. 1 (Color online) **a** STEM-HAADF image of $FeSe_{0.06}S_{0.94}$ with the incident beam along the [001] direction. The [001] projection of the structure model is illustrated with yellow and green spheres representing Fe and Se/S atom, respectively. Scale bar 1nm. **b** Intensity profile (black circles in top) from the white dash scan line shown in (**a**). Two other intensity profiles from images of $FeSe_{0.31}S_{0.69}$ and $FeSe_{0.82}S_{0.18}$ are shown in green and red circles, respectively. The solid lines are the fitted curves based on Gaussian function to obtain the full width at half maximum (FWHM) of Fe and Se/S columns. **c** Normalized FWHM of Se/S columns ($FWHM_{Se/S}/FWHM_{Fe}$) as a function to S concentration x in $FeSe_{1-x}S_x$. **d**, **e** Temperature dependence of in-plane resistivity ρ(T) for $FeSe_{1-x}S_x$. Inset in **d** shows the $d\rho/dT$ versus T for the indicated samples. Inset in e shows the resistivity upturn region in $\log_{10}T$ scale for $x = 0.4$. **f**, **g** The enlargement of superconducting transitions at low temperatures

FeS crystals [70–72]. Crystals obtained by hydrothermal technique usually contain more impurities, however crystals near $x = 0.5$ and $x = 1$ crystal are created using the same hydrothermal crystal growth. Whereas $x = 0.4$ and $x = 0.7$ have low RRR, $x = 1$ has much higher RRR. Indeed, it was observed that FeS is a very good metal with low defect scattering and it shows quantum oscillations just like FeSe crystals made by cvt method [73, 74]. This suggests that the differences observed as x is varied between 0 and 1 are unrelated to synthesis process-related disorder. We note that an anomalous resistivity upturn with a characteristic temperature T^* emerges for $0.3 < x < 0.7$ as observed in our previous work [63, 64], similar in $FeSe_{1-x}S_x$ thin films [75]. Below $T^* \sim 18$ K for a representative sample $x = 0.4$ (inset in Fig. 1e), the resistivity obeys a $\log_{10}T$-dependence before T_c, which might be related to spin fluctuations caused by strong nanoscale crystallographic disorder [35]. Figure 1(f,g) shows the ρ(T) curves at low temperatures for $FeSe_{1-x}S_x$; an abrupt resistivity drop can be clearly seen, signaling the onset of SC. Zero resistivity is observed at $T_c = 9.3(1)$ K for FeSe; the T_c shows a maximum value of 10.6(1) K for $x = 0.12$ within the nematic region, a minimum value of 2.1(1) K for $x = 0.4$, and increases again to $\sim$ 4.5(1) K for FeS [Table 1]. This two-dome-like superconducting phase diagram of $FeSe_{1-x}S_x$ was plotted in our previous work [63, 64], and similar feature was also observed in several other unconventional superconductors [76–79].

Figure 2a presents the magnetic field dependence of Hall resistivity ρ_{xy} at $T = 10$ K for $FeSe_{1-x}S_x$. A strong nonlinear feature is observed for FeSe, and it is gradually weakened with increasing x in high-Se region. Linear field dependence of ρ_{xy} is seen for $x = 0.4$ and 0.7, and then it evolves into nonlinear again for high-S samples, confirming multi-band and delicate tuning in carriers. The Hall effect is dominated by hole carriers at high fields with a change of sign at low fields for $x \leq 0.12$; the sign change is absent for higher x samples (inset in Fig. 2a). We should note that the low-field negative Hall coefficients in CVT-grown FeSe, arising from a small minority of highly mobile electron carriers [80–82], was not observed in hydrothermal FeSe [36], due to more disorder induced by hydrothermal method. With increasing x, the Hall effect is dominated by electron carriers for high-S hydrothermal samples. Figure 2(b) shows the ρ_{xy} curves at $T = 100$ K with linear-field dependence for all samples; the slope is positive with slight change for $0 \leq x \leq 0.23$, confirming isovalent S substitution, which changes into negative with dominant electrons for high-S hydrothermal samples. Figure 2(c-e) displays the temperature-dependent Hall coefficient R_H with error bars determined from linear fits of ρ_{xy} below 1 T for $FeSe_{1-x}S_x$. Within the nematic region $0 \leq x < 0.17$ (Fig. 2c), the R_H shows a W-shape in T-dependence and changes in sign several times, reflecting multi-band nature. The values of R_H are small at high temperatures, which can be understood by a compensated multi-band model. The sign change of R_H above 100 K (Fig. 2c inset, T_1 and T_2) suggests that at some temperatures the holes are more mobile and at other temperatures the electrons are. With decreasing

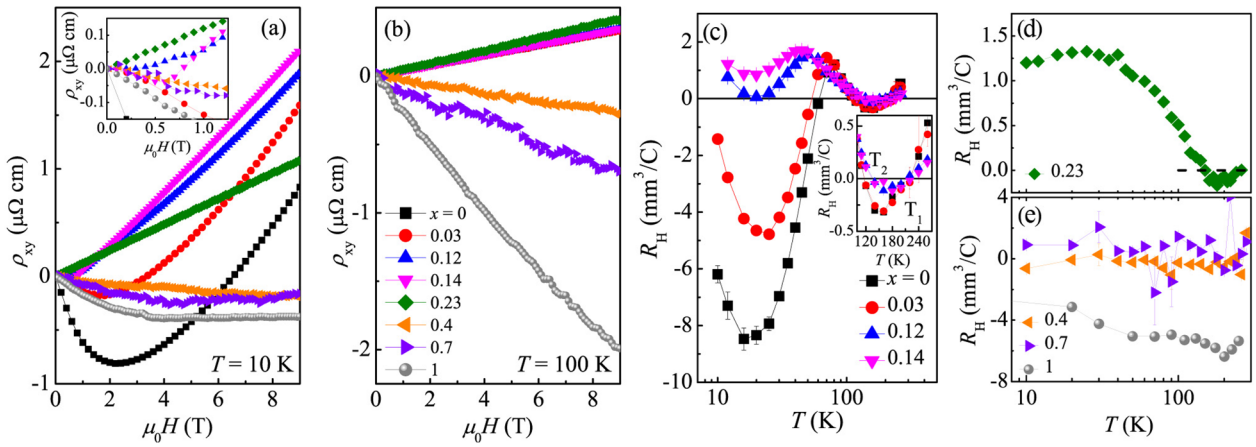

Fig. 2 (Color online) Field dependence of Hall resistivity ρ_{xy} at representative temperatures **a** $T = 10$ K and **b** $T = 100$ K for $FeSe_{1-x}S_x$. Inset in a shows the low-field data for the indicated samples. **c**–**e** Temperature dependence of low-field Hall coefficient R_H for $FeSe_{1-x}S_x$

temperature, a humplike feature was observed with its peak temperature gradually suppressed by S substitution, corresponding to the suppressed nematic transition. The R_H decreases below the peak temperature due to an enhanced contribution of electron-type carriers which becomes dominant for $x = 0$ and 0.03 while it stays positive for $x = 0.12$ and 0.14; then it increases again below 20 K. Across the NCP, the behavior is clearly different for higher x. For $x = 0.23$ (Fig. 2d), the R_H also changes in sign twice at high temperatures but it gradually increases and saturates at ~ 1.25 mm^3/C below 30 K. The values of R_H are of the same order or smaller for $x = 0.4$ and 0.7 (Fig. 2e) with weak temperature dependence when compared to $x = 0.23$, however, it is not clear about the sign change due to larger error bars. This roughly points to larger values of carrier density in hydrothermal-grown $x = 0.4$ and 0.7. For FeS, the R_H is negative in the whole temperatures range, in agreement with previous report [72].

Figure 3(a,b) shows the temperature dependence of in-plane thermopower. For FeSe, the S(T) is positive $\sim$ 18 μV/K at 300 K, changes sign at 215 K, goes through a broad negative minimum $\sim$ -30 μV/K at 110 K, and changes sign again below $\sim$ 15 K, similar to the reported features in polycrystalline FeSe [83–85]. This is indicative of a multiband system with competition of almost compensated hole and electron bands. At high temperatures, the positive values of S(T) dominated by hole band are almost unchanged with x within the nematic region (Fig. 3a), confirming that the effect of S substitution is in chemical pressure rather than in charge carrier doping. With decreasing temperature, the S(T) changes sign at 190 $\sim$ 215 K for $x = 0$ - 0.14, corresponding to the first sign change of R_H at T_1 (Fig. 2c inset); the T_{min} for minima thermpower (defined by $dS/dT = 0$ in Fig. 3a inset) shifts from 110 to 145 K with increasing x, agreeing well with the second sign change at T_2 in R_H (Fig. 2c inset) [80, 81].

Interestingly, a weak hump-like feature occurs around $T_{hump} \sim 45(5)$ K defined by the local maximum in dS/dT for FeSe (Fig. 4a inset); it is rather weak for $x = 0.03$ and becomes more apparent at $T_{hump} \sim 64(2)$ K and 51(1) K for $x = 0.12$ and 0.14, respectively, when RRR is decreased. The T_{hump} is close to the T_s for $x = 0.12$ and 0.14, but if it is due to the nematic transition it should be more apparent in undoped FeSe at $T_s \sim 89$ K, which is not seen here. If we consider the local minimum in dS/dT as the onset temperature of the hump, it is enhanced from 74(3) K for $x = 0$ to 88(11) K for $x = 0.14$, in contrast to the suppression of nematic transition with increasing S substitution. Additionally, it would not be pure carrier diffusion effect that would also produce more apparent feature for $x = 0$ and 0.03 due to pronounced variation in R_H when compared to $x = 0.12$ and 0.14 (Fig. 2c). In the temperature-dependent angle-resolved photoemission spectroscopy (ARPES) measurements of detwinned FeSe, the disappearance of a band can be inferred at this particular energy at $T \sim 60$ K [86], i.e. a Lifshitz transition as a function of temperature in FeSe [28]. However, we can not exclude the phonon drag effect although there is no peak at $\Theta_D/5 \sim 44.6(2)$ K with the Debye temperature $\Theta_D = 223(1)$ K for FeSe (see below). In addition, DFT and DMFT calculations of pressurized FeSe predict two topological transitions [87]. With S substitution, there is strong increase in the interlayer warping in $FeSe_{1-x}S_x$, as the conducting layers come closer together due to chemical pressure, yet we also note the presence of disorder as evidenced in decreased RRR. The high-resolution ARPES detected a small inner hole pocket for $x = 0.12$, which is pushed below the Fermi level in pure FeSe [66].

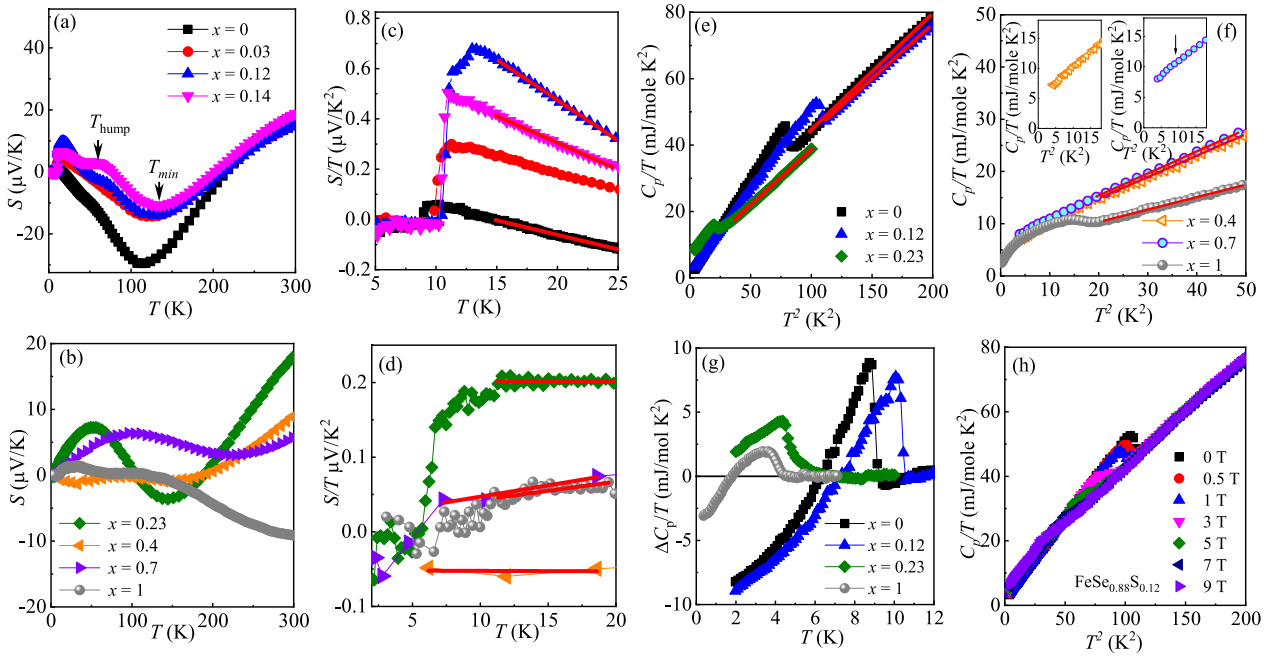

Fig. 3 (Color online) **a**, **b** Temperature dependence of in-plane thermopower *S*(T) for $FeSe_{1-x}S_x$. Inset in a shows the *dS*/*dT* versus *T* curves with arrows defining T_{hump} and T_{min}, respectively. **c**, **d** The *S*/*T* versus *T* curves at low temperatures with linear fits before T_c. **e**, **f** Temperature dependence of specific heat C_p/T vs T^2 with linear fits above T_c for $FeSe_{1-x}S_x$. **g** The $\Delta C_p/T$ versus *T* subtracted by the linear fit for the indicated samples. **h** The C_p/T versus T^2 at various fields for $FeSe_{0.88}S_{0.12}$. Inset in (h) shows the field induced electronic specific heat $\Delta\gamma_e$ versus $\mu_0 H$ with a fit to the Volovik relation $\Delta\gamma_e = A\sqrt{H}$

Table 1 A set of parameters derived from in-plane resistivity ρ(T), thermopower *S*(T), and specific heat C_p(T) with errors from fitting or calculation for $FeSe_{1-x}S_x$

x	T_s (K)	T_c (K)	*S*/*T* (μV/K^2)	T_F (×10^3 K)	T_c/T_F (×10^{-3})	γ (mJ/mol K^2)	Θ_D (K)	λ	*q*	m^* (×m_e)	k_F (1/nm)	v_F (km/s)
0	89(1)	9.3(1)	0.169(3)	2.52(5)	3.69(3)	9.5(3)	223(1)	0.91(2)	1.72(2)	6.4(1)	6.03(3)	109(1)
0.03	82(1)	9.9(1)	0.459(4)	0.93(1)	10.6(1)							
0.12	65(1)	10.6(1)	1.118(5)	0.38(1)	27.6(5)	11.0(2)	228(1)	0.97(2)	9.8(1)	13.4(1)	3.39(2)	29(1)
0.14	61(2)	10.5(1)	0.730(6)	0.58(1)	18.3(1)							
0.23		5.2(1)	0.201(6)	2.12(6)	2.45(2)	5.2(1)	226(1)	0.71(2)	3.73(4)	4.6(1)	4.70(2)	118(2)
0.4		2.1(1)	-0.05(1)	8.5(17)	0.25(4)	6.7(2)	212(1)	0.56(2)	0.7(1)	3.5(1)	8.2(1)	202(4)
0.7		3.7(1)	0.017(8)	25(12)	0.15(7)	7.0(1)	210(1)	0.65(2)	0.2(1)	2.5(1)	12(2)	556(70)
1		4.5(1)	0.018(7)	24(10)	0.19(7)	5.5(1)	254(1)	0.65(2)	0.3(1)	2.2(1)	11(1)	579(26)

The Shubnikov-de Haas oscillation experiment shows a sudden change in extremal areas of Fermi surface pockets near $x \sim 0.15$ [45], i.e. a S-substitution-induced Lifshitz transition that is generated by a sizeable nonlocal Fe d_{xy} nematic term at the corner of the Brillouin zone [28]. The S-substitution-induced Lifshitz transition with $x \sim 0.12$ - 0.15 explains a more visible hump feature in the *S*(T) when compared to FeSe. Therefore, we propose the S-substitution-induced Lifshitz transition possibly plays a role for the pronounced hump in *S*(T) for $x = 0.12$ and 0.14, perhaps combined with the phonon drag effect. Moreover Lifshitz transition associated with sharp changes in the Fermi surface should be facilitated with the nematic order suppression, in line with our observatons [28], whereas disorder effects from sulfur substitution (Fig. 1a–c) should decrease phonon drag contribution [88]. We should note that the ARPES detecteition between 180 and 282 K for $FeSe_{0.945}S_{0.055}$ [89] is not reflected in our thermopower measurement for $x = 0.03$. Outside the nematic region, the value of

S(300 K) decreases with increasing x and finally becomes a negative value of ~ -9 μV/K for FeS Fig. 3b, in line with its negative value of R_H.

Figure 3c, d shows the temperature-dependent S/T at low temperatures. Linear T-dependence observed above T_c sharply decreases to zero below T_c, and the values of T_c agrees with the resistivity results. Zero-temperature extrapolations of S/T are summarized in Table 1. The thermopower S is usually given by [90–94],

$$\frac{S}{T} = \pm\frac{\pi^2}{2}\frac{k_B}{e}\frac{1}{T_F} = \pm\frac{\pi^2}{3}\frac{k_B^2}{e}\frac{N(\varepsilon_F)}{n}, \quad (1)$$

where e is the electron charge, k_B is the Boltzmann constant, T_F is the Fermi temperature related to the Fermi energy ε_F and density of states $N(\varepsilon_F)$ as $N(\varepsilon_F) = 3n/2\varepsilon_F = 3n/2k_BT_F$, and n is the carrier concentration. In a multiband system, it gives the upper limit of T_F of dominant band. Therefore we can extract $T_F = 2.52(5) \times 10^3$ K for FeSe, decreases to $0.38(1) \times 10^3$ K for $x = 0.12$ and then increases to $2.03(6) \times 10^3$ K for $x = 0.23$ [Table 1]. The ratio of T_c/T_F typically characterizes the correlation strength in superconductors. For example, the T_c/T_F is close to 0.1 in $Fe_{1+y}Te_{1-x}Se_x$ [49], pointing to the importance of electronic correlation, while it is ~ 0.02 in a BCS superconductor $LuNi_2B_2C$ [49]. The value of T_c/T_F is ~ 0.0276(5) for $FeSe_{0.88}S_{0.12}$, indicating modest correlations, comparable to $K_xFe_{2-y}Se_2$ ~ 0.04 [52]. Moreover, the derived values of T_c/T_F [Table 1] show a significant reduction in electronic correlations across the NCP for higher x samples.

Figure 3(e,f) shows the heat capacity C_p/T as a function of T^2 in zero field. A clear jump is observed at T_c, in agreement with the transport measurements, indicating bulk SC except for $x = 0.4$ where resistivity reaches zero just below 2 K (Fig. 1e). The data just above T_c can be well fitted by $C_p/T = \gamma + \beta T^2$, where the first term is the Sommerfeld electronic specific heat coefficient and the second term is low-temperature limit of lattice heat capacity. The derived γ as well as the Debye temperature $\Theta_D = (12\pi^4 NR/5\beta)^{1/3}$, where $N = 2$ is the number of atoms per formula unit, and $R = 8.314$ J mol^{-1} K^{-1} is the molar gas constant, are summarized in Table 1. According to the McMillan formula for electron–phonon mediated SC, the electron–phonon coupling constant λ can be deduced by

$$T_c = \frac{\Theta_D}{1.45}\exp\left[-\frac{1.04(1+\lambda)}{\lambda - \mu^*(1+0.62\lambda)}\right], \quad (2)$$

where $\mu^* \approx 0.13$ is the common value for Coulomb pseudo-potential [95]. By using the $T_c = 9.3(1)$ K and $\Theta_D = 223(1)$ K for FeSe, we obtain $\lambda \approx 0.91(2)$, a typical value of an intermediate-coupled BCS superconductor. However, the specific heat jump at T_c subtracted by the liner fit (Fig. 3g), $\Delta C_p/\gamma T_c \approx 0.92(3)$, is somehow smaller than the weak coupling value of 1.43 [95].

The electronic specific heat can be also expressed as:

$$\gamma = \frac{\pi^2}{2}k_B\frac{n}{T_F} = \frac{\pi^2}{3}k_B^2 N(\varepsilon_F). \quad (3)$$

Combining equations (1) and (3) yields: $S/T = \pm\gamma/ne$, where the units are V K^{-1} for S, J K^{-2} m^{-3} for γ, and m^{-3} for n, respectively. This relation was shown to hold in the $T = 0$ limit for a large variety of materials, even in the presence of strong correlations, including heavy fermion metals and cuprates [92]. Then we can define a dimensionless quantity

$$q = \frac{S}{T}\frac{N_A e}{\gamma}, \quad (4)$$

where $N_A e = 96440$ C/mol is the Faraday constant. The q gives the number of carriers per formula unit [92]. The derived q is ~ 1.72(2) for FeSe, which increases to 9.8(1) for $x = 0.12$ and then decreases to 3.73(4) for $x = 0.23$; the smaller value of q for higher x samples indicates larger numbers of carriers [Table 1]. Given the volume of unit cell ~ 0.078487 nm^3 for FeSe, we obtain the carrier density per volume $n \approx 7.4(1) \times 10^{21}$ cm^{-3} and the Fermi momentum $k_F = (3\pi^2 n)^{1/3} \approx 6.03(3)$ nm^{-1} for FeSe; changing to $n \approx 1.32(2) \times 10^{21}$ cm^{-3} and $k_F \approx 3.39(2)$ nm^{-1} for $x = 0.12$ and $n \approx 3.51(4) \times 10^{21}$ cm^{-3} and $k_F \approx 4.70(2)$ nm^{-1} for $x = 0.23$, respectively. For samples with higher x, the carrier concentration $n \approx 1.85(4) \sim 6(3) \times 10^{22}$ cm^{-3} and $k_F \approx 8.2(1) \sim 12(2)$ nm^{-1} also increase.

The effective mass m^* derived from $k_BT_F = \hbar^2 k_F^2/2m^*$, evolves from 6.4(1) m_e for FeSe to 13.4(1) m_e for $x = 0.12$, then monotonically decrease to 2.2(1) m_e for FeS, consistent with the evolution of correlation strengths with S substitution. The Fermi velocity v_F obtained by using $\hbar k_F = m^* v_F$; it decreases from 109(1) km s^{-1} for FeSe to 29(1) km s^{-1} for $x = 0.12$, and then monotonically increases to 579(26) km s^{-1} for FeS. The quasiparticle mass is larger inside the nematic phase, indicative of a strongly correlated state; it becomes suppressed outside the nematic region. The experimentally observed changes in the FS topology, together with the varying degree of electronic correlations, will change the balance of electronic interactions in multiband $FeSe_{1-x}S_x$. Moreover, similar nanoscale disorder is observed near NCP ($x = 0.18$) and outside it ($x = 0.69$) (Fig. 1c). This suggests that nematic correlations in critical region are only weakly perturbed by atomic bond distance disorder. Furthermore, this may also imply that enhanced scattering associated with Mooij law violation is

associated with magnetic rather than nematic fluctuations away from NCP [64].

Figure 3(h) shows the specific heat under various magnetic fields for $FeSe_{0.88}S_{0.12}$ with the highest $T_c = 10.6(1)$ K [63, 64], where the superconducting anomaly gradually shifts to lower temperatures with lower amplitude. It is clear that normal state specific heat does not depend on the field. Then we derive the field dependence of $\Delta\gamma(H) = [C_p(H)\text{-}C_p(0)]/T$ by extending the low-temperature specific heat to 0 K at different magnetic fields as plotted in Fig. 4d inset. The $\Delta\gamma(H)$ is close to the Volovik relation, namely $\Delta\gamma(H) \propto \sqrt{H}$ [96], indicating the presence of gap nodes in $FeSe_{0.88}S_{0.12}$. However, we can not distinguish whether the gap nodes are induced by the sign change of gap as in a *d*-wave case, or by the accidental nodes as theoretically predicted for FeAs- and FeSe-based superconductors [97]. This calls for further investigation of heavily S-substituted FeSe.

4 Conclusions

In summary, we have comprehensively investigated the transport and thermodynamic properties of $FeSe_{1-x}S_x$ superconductors. The hump feature in thermopower is more pronounced in S-substituted samples $x = 0.12$ and 0.14, revealing an interplay of the increased chemical pressure, disorder and the orbital selective electronic correlations that are strongly suppressed in $FeSe_{1-x}S_x$ across the NCP and are not driven by the nanoscale Se/S atom disorder.

Acknowledgments

Work at Brookhaven National Laboratory is supported by the Office of Basic Energy Sciences, Materials Sciences and Engineering Division, U.S. Department of Energy under Contract No. DE-SC0012704.

Author contributions

YL and AW contributed equally to this work. CP and YL conceived the research and designed the experiment. YL, AW, QD, and CP performed the synthesis and transport, Hall resistivity, thermopower, and heat capacity measurements, and data analysis. LW and YZ contributed STEM measurements and analysis. YL and CP wrote the paper, with contributions from all authors. All authors discussed the results and commented on the manuscript.

Availability of data and materials

The data that support the findings of this study are available from the corresponding author upon reasonable request.

Declarations

Competing interests

The authors declare that they have no competing interests.

Received: 5 August 2023 Accepted: 26 November 2023
Published online: 22 December 2023

References

1. A.I. Coldea, M.D. Watson, The key ingredients of the electronic structure of FeSe. Annu. Rev. Condens. Matter Phys. **9**, 125 (2018)
2. F. Hsu, J. Luo, K. Yeh, T. Chen, T. Huang, P.M. Wu, Y. Lee, Y. Huang, Y. Chu, D. Yan, M. Wu, Superconductivity in the PbO-type structure α-FeSe. Proc. Natl. Acad. Sci. U.S.A. **105**, 14262 (2008)
3. S. Medvedev, T.M. McQueen, I.A. Troyan, T. Palasyuk, M.I. Eremets, R.J. Cava, S. Naghavi, F. Casper, V. Ksenofontov, G. Wortmann, C. Felser, Electronic and magnetic phase diagram of β-$Fe_{1.01}Se$ with superconductivity at 3.67 K under pressure. Nat. Mater. **8**, 630 (2009)
4. T. Terashima, N. Kikugawa, S. Kasahara, T. Watashige, T. Shibauchi, Y. Matasuda, T. Wolf, A.E. Böhmer, F. Hardy, C. Meingast, H.V. Löhneysen, S. Uji, Pressure-induced antiferromagnetic transition and phase diagram in FeSe. J. Phys. Soc. Jpn. **84**, 063701 (2015)
5. J. Guo, S. Jin, G. Wang, S. Wang, K. Zhu, T. Zhou, M. He, X. Chen, Superconductivity in the iron selenide $K_xFe_2Se_2$ ($0 \le x \le 1.0$). Phys. Rev. B **82**, 180520 (2010)
6. E. Dagotto, Colloquium: the unexpected properties of alkali metal iron selenide superconductors. Rev. Mod. Phys. **85**, 849 (2013)
7. M. Burrard-Lucas, D.G. Free, S.J. Sedlmaier, J.D. Wright, S.J. Cassidy, Y. Hara, A.J. Corkett, T. Lancaster, P.J. Baker, S.J. Blundell, S.J. Clarke, Enhancement of superconducting transition temperature of FeSe by intercalation of a molecular spacer layer. Nat. Mater. **12**, 15 (2013)
8. X.F. Lu, N.Z. Wang, H. Wu, Y.P. Wu, D. Zhao, X.Z. Zeng, X.G. Luo, T. Wu, W. Bao, G.H. Zhang, F.Q. Huang, Q.Z. Huang, X.H. Chen, Coexistence of superconductivity and antiferromagnetism in $(Li_{0.8}Fe_{0.2})$OHFeSe. Nat. Mater. **14**, 325 (2015)
9. X. Dong, H. Zhou, H. Yang, J. Yuan, K. Jin, F. Zhou, D. Yuan, L. Wei, J. Li, X. Wang, G. Zhang, Z. Zhao, Phase diagram of $(Li_{1-x}Fe_x)$OHFeSe: a bridge between iron selenide and arsenide superconductors. J. Am. Chem. Soc. **137**, 66 (2015)
10. B. Lei, J.H. Cui, Z.J. Xiang, C. Shang, N.Z. Wang, G.J. Ye, X.G. Luo, T. Wu, Z. Sun, X.H. Chen, Evolution of high-temperature superconductivity from a low-T_c phase tuned by carrier concentration in FeSe thin flakes. Phys. Rev. Lett. **116**, 077002 (2016)
11. C.H. Wen, H.C. Xu, C. Chen, Z.C. Huang, X. Lou, Y.J. Pu, Q. Song, B.P. Xie, M. Abdel-Hafiez, D.A. Chareev, A.N. Vasiliev, R. Peng, D.L. Feng, Anomalous correlation effects and unique phase diagram of electron-doped FeSe revealed by photoemission spectroscopy. Nat. Commun. **7**, 10840 (2016)
12. J.J. Seo, B.Y. Kim, B.S. Kim, J.K. Jeong, J.M. Ok, J.S. Kim, J.D. Denlinger, S.K. Mo, C. Kim, Y.K. Kim, Superconductivity below 20 K in heavily electron-doped surface layer of FeSe bulk crystal. Nat. Commum. **7**, 11116 (2016)
13. R. Sun, S. Jin, J. Deng, M. Hao, X. Zhong, Y. Ma, M. Li, X. Chen, Chemical pressure boost record-high superconductivity in van der Waals materials $FeSe_{1-x}S_x$. Adv. Funct. Mater. **31**, 2102917 (2021)
14. Q.-Y. Wang, Z. Li, W.-H. Zhang, Z.-C. Zhang, J.-S. Zhang, W. Li, H. Ding, Y.-B. Ou, P. Deng, K. Chang, J. Wen, C.-L. Song, K. He, J.-F. Jia, S.-H. Ji, Y.-Y. Wang, L.-L. Wang, X. Chen, X.-C. Ma, Q.-K. Xue, Interface-induced high-temperature superconductivity in single unit-cell FeSe films on $SrTiO_3$. Chin. Phys. Lett. **29**, 037402 (2012)
15. S. Tan, Y. Zhang, M. Xia, Z. Ye, F. Chen, X. Xie, R. Peng, D. Xu, Q. Fan, H. Xu, J. Jiang, T. Zhang, X. Lai, T. Xiang, J. Hu, B. Xie, D. Feng, Interface-induced superconductivity and strain-dependent spin density waves in FeSe/$SrTiO_3$ thin films. Nat. Mater. **12**, 634 (2013)
16. S. He, J. He, W. Zhang, L. Zhao, D. Liu, X. Liu, D. Mou, Y.-B. Ou, Q.-Y. Wang, Z. Li, L. Wang, Y. Peng, Y. Liu, C. Chen, L. Yu, G. Liu, X. Dong, J. Zhang, C. Chen, Z. Xu, X. Chen, X. Ma, Q. Xue, X.J. Zhou, Phase diagram and electronic indication of high-temperature superconductivity at 65 K in single-layer FeSe films. Nat. Mater. **12**, 605 (2013)
17. J.J. Lee, F.T. Schmitt, R.G. Moore, S. Johnston, Y.-T. Cui, W. Li, M. Yi, Z.K. Liu, M. Hashimoto, Y. Zhang, D.H. Lu, T.P. Devereaux, D.-H. Lee, Z.-X. Shen, Interfacial mode coupling as the origin of the enhancement of T_c in FeSe films on $SrTiO_3$. Nature **515**, 245 (2014)
18. J.F. Ge, Z.L. Liu, C. Liu, C.L. Gao, D. Qian, Q.K. Xue, Y. Liu, J.F. Jia, Superconductivity above 100 K in single-layer FeSe films on doped $SrTiO_3$. Nat. Mater. **14**, 285 (2015)

19. T. Shibauchi, T. Hanaguri, Y. Matsuda, Exotic superconducting states in FeSe-based materials. J. Phys. Soc. Jpn. **89**, 102002 (2020)
20. T.M. McQueen, A.J. Williams, P.W. Stephens, J. Tao, Y. Zhu, V. Ksenofontov, F. Casper, C. Felser, R.J. Cava, Tetragonal-to-orthorhombic structural phase transition at 90 K in the superconductor $Fe_{1.01}Se$. Phys. Rev. Lett. **103**, 057002 (2009)
21. S.-H. Baek, D. V. Efremov, J. M. Ok, J. S. Kim, Jeroen van den Brink, B. Büchner, Orbital-driven nematicity in FeSe, Nat. Mater. **14**, 210 (2015)
22. A.E. Böhmer, T. Arai, F. Hardy, T. Hattori, T. Iye, T. Wolf, H.V. Löhneysen, K. Ishida, C. Meingast, Origin of the tetragonal-to-orthorhombic phase transition in FeSe: a combined thermodynamic and NMR study of nematicity. Phys. Rev. Lett. **114**, 027001 (2015)
23. S. Mukherjee, A. Kreisel, P.J. Hirschfeld, B.M. Anderson, Model of electronic structure and superconductivity in orbitally ordered FeSe. Phys. Rev. Lett. **115**, 026402 (2015)
24. A.V. Chubukov, R.M. Fernandes, J.J. Schmalian, Origin of nematic order in FeSe. Phys. Rev. B **91**, 201105(R) (2015)
25. J.K. Glasbrenner, I.I. Mazin, H.O. Jeschke, P.J. Hirschfeld, R.M. Fernandes, R. Valenti, Effect of magnetic frustration on nematicity and superconductivity in iron chalcogenides. Nat. Phys. **11**, 953 (2015)
26. A.I. Coldea, Electronic nematic states tuned by isoelectronic substitution in bulk $FeSe_{1-x}S_x$. Front. Phys. **8**, 594500 (2021)
27. M.D. Watson, T.K. Kim, A.A. Haghighirad, N.R. Davies, A. McCollam, A. Narayanan, S.F. Blake, Y.L. Chen, S. Ghannadzadeh, A.J. Schofield, M. Hoesch, C. Meingast, T. Wolf, A.I. Coldea, Emergence of the nematic electronic state in FeSe. Phys. Rev. B **91**, 155106 (2015)
28. L.C. Rhodes, J. Böker, M.A. Müller, M. Eschrig, I.M. Eremin, Non-local d_{xy} nematicity and the missing electron pocket in FeSe. NPJ Quantum Mater. **6**, 45 (2021)
29. Y. Sun, S. Kittaka, S. Nakamura, T. Sakakibara, K. Irie, T. Nomoto, K. Machida, J. Chen, T. Tamegai, Gap structure of FeSe determined by angle-resolved specific heat measurements in applied rotating magnetic field. Phys. Rev. B **96**, 220505(R) (2017)
30. M.D. Watson, S.F. Blake, A.A. Haghighirad, M. Hoesch, T.K. Kim, A.I. Coldea, R. Valentí, Formation of Hubbard-like bands as a fingerprint of strong electron-electron interactions in FeSe. Phys. Rev. B **95**, 081106(R) (2017)
31. M.A. Hafiez, Y.Y. Zhang, Z.Y. Cao, C.C. Duan, G. Karapetrov, V.M. Pudalov, V.A. Vlasenko, A.V. Sadakov, D.A. Knyazev, T.A. Romanova, D.A. Chareev, O.S. Volkova, A.N. Vasiliev, X.J. Chen, Superconducting properties of sulfur-doped iron selenide. Phys. Rev. B **91**, 165109 (2015)
32. S. Hosoi, K. Matsuura, K. Ishida, H. Wang, Y. Mizukami, T. Watashige, S. Kasahara, Y. Matsuda, T. Shibauchi, Nematic quantum critical point without magnetism in $FeSe_{1-x}S_x$ superconductors. Proc. Natl. Acad. Sci. U.S.A. **113**, 8139 (2016)
33. P. Reiss, M.D. Watson, T.K. Kim, A.A. Haghighirad, D.N. Woodruff, M. Bruma, S.J. Clarke, A.I. Coldea, Suppression of electronic correlations by chemical pressure from FeSe to FeS. Phys. Rev. B **96**, 121103(R) (2017)
34. P. Wiecki, K. Rana, A.E. Böhmer, Y. Lee, S.L. Bud'ko, P.C. Canfield, Y. Furukawa, Persistent correlation between superconductivity and antiferromagnetic fluctuations near a nematic quantum critical point in $FeSe_{1-x}S_x$. Phys. Rev. B **98**, 020507(R) (2018)
35. X. Yi, X. Xing, L. Qin, J. Feng, M. Li, Y. Zhang, Y. Meng, N. Zhou, Y. Sun, Z.X. Shi, Hydrothermal synthesis and complete phase diagrams of $FeSe_{1-x}S_x$ ($0 \leq x \leq 1$) single crystals. Phys. Rev. B **103**, 144501 (2021)
36. W.H. Liu, X.L. Yi, W.C. Li, X.Z. Xing, H.J. Zhao, M.X. Xu, Z.X. Shi, Transport properties and phase diagrams of $FeSe_{1-x}S_x$ ($0 \leq x \leq 1$) single crystals. J. Alloys Compd. **919**, 165760 (2022)
37. S. Lederera, Y. Schattnerb, E. Berg, S.A. Kivelsond, Superconductivity and non-Fermi liquid behavior near a nematic quantum critical point. Proc. Natl. Acad. Sci. U.S.A. **114**, 4905 (2017)
38. S. Licciardello, J. Buhot, J. Hu, J. Ayres, S. Kasahara, Y. Matasuda, T. Shibauchi, N.E. Hussey, Electrical resistivity across a nematic quantum critical point. Nature **567**, 213 (2019)
39. M. Bristow, P. Reiss, A.A. Haghighirad, Z. Zajicek, S.J. Singh, T. Wolf, D. Graf, W. Knafo, A. McCollam, A.I. Coldea, Anomalous high-magnetic field electronic state of the nematic superconductors $FeSe_{1-x}S_x$. Phys. Rev. Research **2**, 013309 (2020)
40. W.K. Huang, S. Hosoi, M. Culo, S. Kasahara, Y. Sato, K. Matsuura, Y. Mizukami, M. Berben, N.E. Hussey, H. Kontani, T. Shibauchi, Y. Matsuda, Non-Fermi liquid transport in the vicinity of the nematic quantum critical point of superconducting $FeSe_{1-x}S_x$. Phys. Rev. Research **2**, 033367 (2020)
41. M. Čulo, M. Berben, Y.-T. Hsu, J. Ayres, R. D. H. Hinlopen, S. Kasahara, Y. Matsida, T. Shibauchi, N. E. Hussey, Putative Hall response of the strange metal component in $FeSe_{1-x}S_x$, Phys. Rev. Res. **3**, 023069 (2021)
42. K. Rana, Y. Furukawa, Relationship between nematicity, antiferromagnetic fluxtuations, and superconductivity in $FeSe_{1-x}S_x$ revealed by NMR. Front. Phys. **10**, 849284 (2022)
43. W. Zhang, S. Wu, S. Kasahara, T. Shibauchi, Y. Matsuda, G. Blumberg, Quadrupolar charge dynamics in the nonmagnetic $FeSe_{1-x}S_x$ superconductors. PNAS **118**, e2020585118 (2021)
44. N. Lazarević, A. Baum, A. Milosavljević, L. Peis, R. Stumberger, J. Bekaert, A. Šolajić, J. Pešić, A. Wang, M. Šćepanović, A.M.M. Abeykoon, M.V. Milošević, C. Petrovic, Z.V. Popović, R. Hackl, Evolution of lattice, spin, and charge properties across the phase diagram of $FeSe_{1-x}S_x$. Phys. Rev. B **106**, 094510 (2022)
45. A.I. Coldea, S.F. Blake, S. Kasahara, A.A. Haghighirad, M.D. Watson, W. Knafo, E.S. Choi, A. McCollam, P. Reiss, T. Yamashita, M. Bruma, S.C. Speller, Y. Matsuda, T. Wolf, T. Shibauchi, A.J. Schofield, Evolution of the low-temperature Fermi surface of superconducting $FeSe_{1-x}S_x$ across a nematic phase transition, npj Quant. Mater. **4**, 2 (2019)
46. A.S. Sefat, M.A. McGuire, B.C. Sales, R. Jin, J.Y. Howe, D. Mandrus, Electronic correlations in the superconductor $LaFeAsO_{0.89}F_{0.11}$ with low carrier density. Phys. Rev. B **77**, 174503 (2008)
47. N. Kang, P. Auban-Senzier, C.R. Pasquier, Z.A. Ren, J. Yang, G.C. Chen, Z.X. Zhao, Pressure dependence of the thermoelectric power of the iron-based high-T_c superconductor $SmFeAsO_{0.85}$. New J. Phys. **11**, 025006 (2009)
48. E. D. Mun, S. L. Bud'ko, Ni Ni, A. N. Thaler, P. C. Canfield, Thermoelectric power and Hall coefficient measurements on $Ba(Fe_{1-x}T_x)_2As_2$ (T = Co and Cu), Phys. Rev. B **80**, 054517 (2009)
49. A. Pourret, L. Malone, A.B. Antunes, C.S. Yadav, P.L. Paulose, B. Fauque, K. Behnia, Strong correlation and low carrier density in $Fe_{1+y}Te_{0.6}Se_{0.4}$ as seen from its thermoelectric response. Phys. Rev. B **83**, 020504(R) (2011)
50. M. Matusiak, T. Plackowski, Z. Bukowski, N.D. Zhigadlo, J. Karpinski, Evidence of spin-density-wave order in $RFeAsO_{1-x}F_x$ from measurements of thermoelectric power. Phys. Rev. B **79**, 212502 (2009)
51. N.P. Butch, S.R. Saha, X.H. Zhang, K. Kirshenbaum, R.L. Greene, J. Paglione, Effective carrier type and field dependence of the reduced-T_c superconducting state in $SrFe_{2-x}Ni_xAs_2$. Phys. Rev. B **81**, 024518 (2010)
52. K. Wang, H. Lei, C. Petrovic, Thermoelectric studies of $K_xFe_{2-y}Se_2$ indicating a weakly correlated superconductor. Phys. Rev. B **83**, 174503 (2011)
53. K. Wang, H. Lei, C. Petrovic, Evolution of correlation strength in $K_xFe_{2-y}Se_2$ superconductor doped with S. Phys. Rev. B **84**, 054526 (2011)
54. C. Collignon, A. Ataei, A. Gourgout, S. Badoux, M. Lizaire, A. Legros, S. Licciardello, S. Wiedmann, J.Q. Yan, J.S. Zhou, Q. Ma, B.D. Gaulin, N. Doiron-Leyraud, L. Taillefer, Thermopower across the phase diagram of the cuprate $La_{1.6-x}Nd_{0.4}Sr_xCuO_4$: Signatures of the pseudogap and charge density wave phases. Phys. Rev. B **103**, 155102 (2021)
55. D. Kim, E.-C. Shin, Y. Lee, Y.H. Lee, M. Zhao, Y.-H. Kim, H. Yang, Atomic-scale thermopower in charge density wave states. Nat. Commun. **13**, 4516 (2022)
56. P.R. Mandal, T. Sarkar, R.L. Greene, Anomalous quantum criticality in the electron-doped cuprates. Proc. Natl. Acad. Sci. U.S.A. **116**, 5991 (2019)
57. S. Badoux, S.A.A. Afshar, B. Michon, A. Ouellet, S. Fortier, D. LeBoeuf, T.P. Croft, C. Lester, S.M. Hayden, H. Takagi, K. Yamada, D. Graf, N. Doiron-Leyraud, L. Taillefer, Critical doping for the onset of Fermi-surface reconstruction by charge-density-wave order in the cuprate superconductor $La_{2-x}Sr_xCuO_4$. Phys. Rev. X **6**, 021004 (2016)
58. O. Cyr-Choinière, S. Badoux, G. Grissonnanche, B. Michon, S.A.A. Afshar, S. Fortier, D. LeBoeuf, D. Graf, J. Day, D.A. Bonn, W.N. Hardy, R. Liang, N. Doiron-Leyraud, L. Taillefer, Anisotropy of the Seebeck coefficient in the cuprate superconductor $YBa_2Cu_3O_y$: Fermi-surface reconstruction by bidirectional charge order. Phys. Rev. X **7**, 031042 (2017)
59. S.L. Skornyakov, A.I. Leonov, Correlated electronic structure, orbital-dependent correlations and Lifshitz transition in tetragonal FeS. Phys. Rev. B **100**, 235123 (2019)
60. A. Wang, L. Wu, V.N. Ivanovski, J.B. Warren, J. Tian, Y. Zhu, C. Petrovic, Critical current density and vortex pinning in tetragonal $FeS_{1-x}Se_x$ (x = 0, 0.06). Phys. Rev. B **94**, 094506 (2016)
61. A. Wang, C. Petrovic, Vortex pinning and irreversibility fields in $FeS_{1-x}Se_x$ (x = 0, 0.06). Appl. Phys. Lett. **110**, 232601 (2017)
62. Y. Liu, A. Wang, V.N. Ivanovski, Q. Du, V. Koteski, C. Petrovic, Thermoelectricity and electronic correlation enhancement in FeS by light Se doping. Phys. Rev. B **105**, 045133 (2022)

63. A. Wang, A. Milosavljevic, A.M.M. Abeykoon, V. Ivanovski, Q. Du, A. Baum, E. Stavitski, Y. Liu, N. Lazarevic, K. Attenkofer, R. Hackl, Z. Popovic, C. Petrovic, Suppression of superconductivity and nematic order in $Fe_{1-y}Se_{1-x}S_x$ ($0 \leq x \leq 1, y \leq 0.1$) crystals by anion height disorder. Inorg. Chem. **61**, 11036 (2022)
64. A. Wang, L. Wu, Q. Du, M. Naamneh, W.H. Brito, A.M.M. Abeykoon, W.R. Pudelko, J. Jandke, Y. Liu, N.C. Plumb, G. Kotliar, V. Dobrosavljevic, M. Radovic, Y. Zhu, C. Petrovic, Mooij law violation from nanoscale disorder. Nano Lett. **22**, 6900 (2022)
65. A. Wang, C. Petrovic, Electron correlations in the H_{c2} of $Fe_ySe_{1-x}S_x$ ($0.10 \leq x \leq 0.24, y \geq 0.9$). Supercond. Sci. Technol. **35**, 115002 (2022)
66. M.D. Watson, T.K. Kim, A.A. Haghighirad, S.F. Blake, N.R. Davies, M. Hoesch, T. Wolf, A.I. Coldea, Suppression of orbital ordering by chemical pressure in $FeSe_{1-x}S_x$. Phys. Rev. B **92**, 121108(R) (2015)
67. A.E. Böhmer, V. Taufour, W.E. Straszheim, T. Wolf, P.C. Canfield, Variation of transition temperatures and residual resistivity ratio in vapor-grown FeSe. Phys. Rev. B **94**, 024526 (2016)
68. S. Kasahara, T. Watashige, T. Hanaguri, Y. Kohsaka, T. Yamashita, Y. Shimoyama, Y. Mizukami, R. Endo, H. Ikeda, K. Aoyama, T. Terashima, S. Uji, T. Wolf, H.V. Löhneysen, T. Shibauchi, Y. Matsuda, Field-induced superconducting phase of FeSe in the BCS-BES cross-over. PNAS **111**, 16309 (2014)
69. Y. Sun, S. Kittaka, S. Nakamura, T. Sakakibara, K. Irie, T. Namoto, K. Machida, J. Chen, T. Tamegai, Gap structure of FeSe determined by angle-resolved specific heat measurements in applied rotating magnetic field. Phys. Rev. B **96**, 220505(R) (2017)
70. X. Lai, H. Zhang, Y. Wang, X. Wang, X. Zhang, J. Lin, F. Huang, Observation of superconductivity in tetragonal FeS. J. Am. Chem. Soc. **137**, 10148 (2015)
71. C.K.H. Borg, X. Zhou, C. Eckberg, D.J. Campbell, S.R. Saha, J. Paglione, E.E. Rodriguez, Strong anisotropy in nearly ideal tetrahedral superconducting FeS single crystals. Phys. Rev. B **93**, 094522 (2016)
72. H. Lin, Y. Li, Q. Deng, J. Xing, J. Liu, X. Zhu, H. Yang, H.H. Wen, Multiband superconductivity and large anisotropy in FeS crystals. Phys. Rev. B **93**, 144505 (2016)
73. T. Terashima, N. Kikugawa, H. Lin, X. Zhu, H.-H. Wen, T. Nomoto, K. Suzuki, H. Ikeda, S. Uji, Upper critical field and quantum oscillations in tetragonal superconducting FeS. Phys. Rev. B **94**, 100503 (2016)
74. T. Terashima, N. Kikugawa, A. Kiswandhi, E.-S. Choi, J. Brooks, S. Kasahara, T. Watashige, H. Ikeda, T. Shibauchi, Y. Matsuda, T. Wolf, A.E. Bohmer, F. Hardy, C. Meingast, H.V. Lohneysen, M. Suzuki, R. Arita, S. Uji, Anomalous Fermi surface in FeSe seen by Shubnikov-de-Haas oscillation measurements. Phys. Rev. B **90**, 144517 (2014)
75. F. Nabeshima, T. Ishikawa, K. Oyanagi, M. Kawai, A. Maeda, Growth of superconducting epitaxial films of sulfur substituted FeSe via pulsed laser deposition. J. Phys. Soc. Jpn. **87**, 073704 (2018)
76. T. Das, C. Panagopoulos, Two types of superconducting domes in unconventional superconductors. New J. Phys. **18**, 103033 (2016)
77. L. Li, X. Deng, Z. Wang, Y. Liu, M. Abeykoon, E. Dooryhee, A. Tomic, Y. Huang, J.B. Warren, E.S. Bozin, S.J.L. Billinge, Y. Sun, Y. Zhu, G. Kotliar, C. Petrovic, Superconducting order from disorder in 2H-$Ta_{2-x}Se_x$,. NPJ Quant. Mater. **2**, 11 (2017)
78. C.C. Zhu, X.F. Yang, W. Xia, Q.W. Yin, L.S. Wang, C.C. Zhao, D.Z. Dai, C.P. Tu, B.Q. Song, Z.C. Tao, Z.J. Tu, C.S. Gong, H.C. Lei, Y.F. Guo, S.Y. Li, Double-dome superconductivity under pressure in the V-based kagome metals AV_3Sb_5 (A = Rb and K). Phys. Rev. B **105**, 094507 (2022)
79. K.Y. Chen, N.N. Wang, Q.W. Yin, Y.H. Gu, K. Jiang, Z.J. Tu, C.S. Gong, Y. Uwatoko, J.P. Sun, H.C. Lei, J.P. Hu, J.G. Cheng, Double superconducting dome and triple enhancement of T_c in the Kagome superconductor CsV_3Sb_5 under high pressure. Phys. Rev. Lett. **126**, 247001 (2021)
80. M.D. Watson, T. Yamashita, S. Kasahara, W. Knafo, M. Nardone, J. Béard, F. Hardy, A. McCollam, A. Narayanan, S.F. Blake, T. Wolf, A.A. Haghighirad, C. Meingast, A.J. Schofield, H.V. Löhneysen, Y. Matsuda, A.I. Coldea, T. Shibauchi, Dichotomy between the hole and electron behavior in multiband superconductor FeSe probed by ultrahigh magnetic fields. Phys. Rev. Lett. **115**, 027006 (2015)
81. Y. Sun, S. Pyon, T. Tamegai, Electron carriers with possible Dirac-cone-like dispersion in $FeSe_{1-x}S_x$ ($x = 0$ and 0.14) single crystals triggered by structural transition. Phys. Rev. B **93**, 104502 (2016)
82. K.K. Huynh, Y. Tanabe, T. Urata, H. Oguro, S. Heguri, K. Watanabe, K. Tanigaki, Electric transport of a single-crystal iron chalcogenide FeSe superconductor: evidence of symmetry-breakdown nematicity and additional ultrafast Dirac cone-like carriers. Phys. Rev. B **90**, 144516 (2014)
83. Y.J. Song, J.B. Hong, B.H. Min, Y.S. Kwon, K.J. Lee, M.H. Jung, J.S. Rhyee, Superconducting properties of a stoichiometric FeSe compound and two anomalous features in the normal state. J. Korean Phys. Soc. **59**, 312 (2011)
84. F. Caglieris, F. Ricci, G. Lamura, A. Martinelli, A. Palenzona, I. Pallecchi, A. Sala, G. Profeta, M. Putti, Theoretical and experimental investigation of magnetotransport in iron chalcogenides. Sci. Technol. Adv. Mater. **13**, 054402 (2012)
85. K. Onar, M.E. Yakinci, Solid state synthesis and characterization of bulk β -FeSe superconductors. J. Alloy. Compd. **620**, 210 (2015)
86. M. Yi, H. Pfau, Y. Zhang, Y. He, H. Wu, T. Chen, Z.R. Ye, M. Hashimoto, R. Yu, Q. Si, D.-H. Lee, P. Dai, Z.-X. Shen, D.H. Lu, R.J. Birgeneau, Nematic energy scale and the missing electron pocket in FeSe. Phys. Rev. X **9**, 041049 (2019)
87. S. Mandal, R.E. Cohen, K. Haule, Strong pressure-dependent electron-phonon coupling in FeSe. Phys. Rev. B **89**, 220502(R) (2014)
88. Q. Du, L. Wu, H. Cao, C.-J. Kang, C. Nelson, G.L. Pascut, T. Besara, T. Siegrist, K. Haule, G. Kotliar, I. Zaliznyak, Y. Zhu, C. Petrovic, Vacancy defect control of colossal thermopower in FeSb2. npj. Quantum Mater. **6**, 13 (2021)
89. M.A. Hafiez, Y.J. Pu, J. Brisbois, R. Peng, D.L. Feng, D.A. Chareev, A.V. Silhanek, C. Krellner, A.N. Vasiliev, X.J. Chen, Impurity scattering effects on the superconducting properties and the tetragonal-to-orthorhombic phase transition in FeSe. Phys. Rev. B **93**, 224508 (2016)
90. R.D. Barnard, *Thermoelectricity in metals and alloys* (Taylor & Francis, London, 1972)
91. J.L. Cohn, S.A. Wolf, V. Selvamanickam, K. Salama, Thermoelectric power of $YBa_2Cu_3O_{7-\delta}$: Phonon drag and multiband conduction. Phys. Rev. Lett. **66**, 1098 (1991)
92. K. Behnia, D. Jaccard, J. Flouquet, On the thermoelectricity of correlated electrons in the zero-temperature limit. J. Phys. Condens. Matter. **16**, 5187 (2004)
93. K. Miyake, H. Kohno, Theory of quasi-universal ratio of seebeck coefficient to specific heat in zero-temperature limit in correlated metals. J. Phys. Soc. Jpn. **74**, 254 (2005)
94. S. Jiang, H.S. Jeevan, J. Dong, P. Gegenwart, Thermopower as a sensitive probe of electronic nematicity in iron pnictides. Phys. Rev. Lett. **110**, 067001 (2013)
95. W.L. McMillan, Transition temperature of strong-coupled superconductors. Phys. Rev. **167**, 331 (1968)
96. J. Xing, H. Lin, Y. Li, S. Li, X. Zhu, H. Yang, H.H. Wen, Nodal superconducting gap in tetragonal FeS. Phys. Rev. B **93**, 104520 (2016)
97. P. Hrischfeld, M. Korshunov, I. Mazin, Gap symmetry and structure of Fe-based superconductors. Rep. Prog. Phys. **74**, 124508 (2011)

Publisher's Note